Jurnal Ilmu Fisika
Vol. 17, No. 2, September 2025, pp. 182–192
ISSN: 1979-4657 (Print); 2614-7386 (Online)
https://doi.org/10.25077/jif.17.2.182-192.2025

Jurnal Ilmu Fisika
Open Access

Visualization of Ultrasonic Beam from a Medical Transducer using a Combination of Background-Oriented Schlieren Imaging with Hilbert Transformation

Margi Sasono*, Apik Rusdiarna IP

Advanced Laboratory of Physics (AloP), Study Program of Physics, Faculty of Applied Sciences and Technology (FAST)
Ahmad Dahlan University, Yogyakarta, 55166, Indonesia

Article Info

Article History:

Received May 27, 2025
Revised July 06, 2025
Accepted July 31, 2025
Published online August 07, 2025

Keywords:

Visualization
Ultrasonic
Fringe Patterns
Schlieren Imaging
Hilbert Transformation

Corresponding Author:

Margi Sasono,
Email: margi.sasono@fisika.uad.ac.id

ABSTRACT

Ultrasonics in the medical field require a safe treatment for patients. The uncontrolled intensities of the ultrasonic waves cause ineffective treatment. So far, the hydrophone probe provides a standard for ultrasonic visualization. However, this method has constraints such as being time-consuming, intrusive, and requiring off-axis measurements. In this paper, an optical method called background-oriented schlieren imaging (BOSI) has been developed as an alternative. The BOSI uses a background of fringe patterns captured by a digital camera. The ultrasonic waves in water displace the patterns relative to the reference. A Hilbert Transform (HT) has been used to estimate the displacement of patterns proportional to the phase difference. The developed BOSI reconstructs these phase differences as an ultrasonic visualization. This paper reports that the developed BOSI is capable of visualizing the ultrasonic waves produced by a 1-MHz frequency medical transducer operated in continuous-wave (CW) mode. The visualization shows an undulation of phase difference that corresponds to the change in water density due to ultrasonic exposure. Meanwhile, the amplitude mode is proportional to the ultrasonic intensity profile. Thus, the developed BOSI is promising to be used as a calibration device to ensure safe ultrasonics in the medical field.

1. INTRODUCTION

Visualization of the ultrasonic beam is essential in ensuring safety aspects in medical applications such as diagnosis (Akiyama, 2020), therapeutic (Draper and M Mallipudi, 2020), and surgery (Hofmann et al., 2023). In the metrology field, hydrophone scanning has provided a gold standard method to visualize the ultrasonic beam of a medical transducer according to the standard of ISO/IEC 61689:2022 (Harris et al., 2023). However, several issues, including intrusive methods, off-axis measurement, and time-consuming, hamper its widespread use in metrology (Xing et al., 2021). As an alternative, the optical method-based schlieren imaging has been found to be commercially useful in the visualization of ultrasonic beams (Dunlap et al., 2020). However, this device also has several drawbacks, such as the need for precise optical component alignment, a limited field of view (FOV),

and low sensitivity to the acousto-optics effect (Xing et al., 2021). Schlieren imaging is still not a standard in ultrasonic beam metrology.

On the other hand, background-oriented schlieren imaging (BOSI) is a variant of schlieren imaging. Unlike schlieren imaging, the BOSI setup is simple and requires only a background pattern and a digital camera. The visualization technique relies on the change in density of a schlieren object (object under test). A digital camera captures this change as a distorted background pattern to visualize the physical characteristics of the schlieren object. Hence, the BOSI has recently found a wide range of applications, including the qualitative visualization of fluid flow (Yamagishi et al., 2021), aerodynamics (Ding et al., 2019), shock waves (Mizukaki et al., 2020), and many others. In its development, the BOSI has enabled quantitative measurement of refractive index (Grauer and Steinberg, 2020) and medium density (density of a schlieren object) (Kaneko et al., 2021).

An ultrasonic beam can be visible using the BOSI technique (Colom et al., 2023; Koponen et al., 2022; Ichihara et al., 2025). In principle, the propagation of ultrasonic waves in water, for example, can cause a change in the refractive index due to changes in the density of water. If the light rays propagating from the background pattern pass through the refractive index variations, an acousto-optics effect will occur (Shen et al., 2021). A digital camera in the BOSI setup records this effect as a distorted pattern image that contains information about the ultrasonic beam. Therefore, the type of background pattern and image processing method used in the BOSI technique is very important for improving the visualization of ultrasonic waves. Pulkkinen et al. (2017) and Koponen et al. (2022) use a high-power light-emitting diode (LED) driven in pulsating mode as the background and optical flow analysis as image processing. Luo et al. (2020) have developed a continuous-wave background-oriented schlieren (CW-BOS) imaging with a bed-of-nails as background and a multi-layer deep neural network to reconstruct two-dimensional ultrasonic images. Meanwhile, Ichihara et al. (2025) use a checkerboard as the background combined with a Fast Fourier Transform method in image processing. Generally, the BOSI technique uses a combination of random dot patterns with digital image correlation (DIC) as an image processing algorithm (Sasono et al., 2023). However, the distribution of dots on the background plane can be uneven, and the large density changes in the medium (schlieren object) can distort the shape of the dots (Meinecke et al., 2020). Therefore, in recent years, the BOSI technique has considered periodic patterns as the background (Vinnichenko et al., 2023).

This paper proposes a new development of the BOSI technique by using fringe patterns (instead of random dots) as the background, combined with Hilbert Transform (HT) as the image processing method to visualize the ultrasonic beam shape emitted by medical (therapeutic) transducers. This work relies on the principle that ultrasonic waves cause density changes that correspond to the refractive index in water. The background in the BOSI technique is designed as a light source modulated by periodic fringe patterns. The patterns of light source from the background are deflected as they pass through the variations in the refractive index of water, and this situation generates phase-modulated light rays. A digital camera detects this deflection and captures it as a displacement in the fringe pattern. Therefore, this paper proposes a technique using HT to extract the phase of the modulated light rays (phase demodulation) in the visualization of the ultrasonic beam. In the BOSI technique, the phase modulation of light can be explored from the displacement of the fringe patterns in the background. On the other hand, previous studies have shown that fringe patterns outperform random dots as a background to improve BOSI measurements (Vinnichenko et al., 2023). In addition, the phase demodulation technique using HT has been proven accurate for designing phase microscopy devices (Nienhaus et al., 2023). Through the new development of using these fringe patterns to visualize the shape of ultrasonic beams, the developed BOSI can improve ultrasonic calibration methods. For example, in the medical field, knowledge of the shape of ultrasonic beams is important to ensure accuracy in controlling ultrasonic intensity.

2. METHOD

The principle of the BOSI technique is straightforward optically, as seen in Figure 1. The distance between the camera lens and the background patterns is Z, assuming that the value of is much

greater than the focal length of the lens f used ($Z > f$). This arrangement allows parallel light rays along the z-axis (optical axis) by assuming that the background position of the digital camera is infinite (Raffel, 2015). The position of the schlieren object (the refractive index variation in this work) is from the background, located between the background and the digital camera. A light ray from the fringe pattern's background travels to the digital camera through the schlieren object. A mathematical model can describe a light ray path in the schlieren object along the z-axis as (Wei et al., 2021)

$$\frac{d^2y}{dz^2} = \frac{1}{n}\left(\frac{dn}{dy}\right), \tag{1}$$

where n is the refractive index, and (dn/dy)) represents refractive index variations (or refractive index gradient) of a schlieren object under test. Equation (1) states the curvature of a deflected ray in proportion to the strength of the refractive index gradient. As shown in Figure 1, a reference light ray has no deflection toward the digital camera. The changes in the refractive index lead to a light ray deflection, as depicted by the solid lines in Figure 1. The digital camera captures this deflection as a displacement in the position of the light ray incident on the image plane of the digital camera.

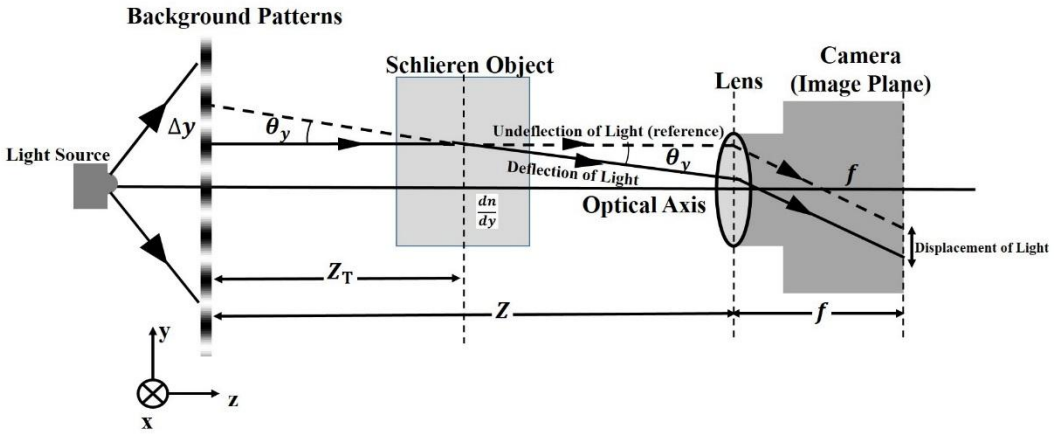

Figure 1. Schematic diagram of the principle of BOSI.

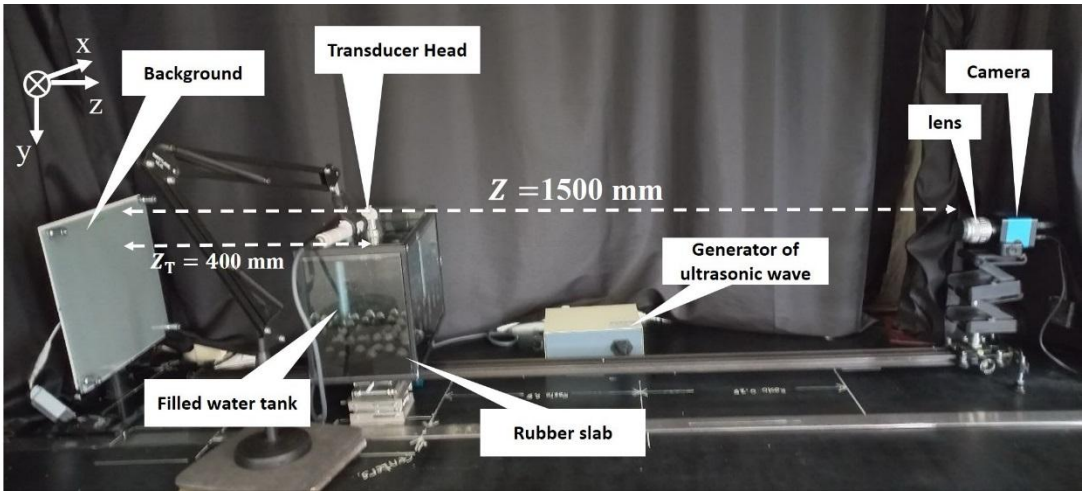

Figure 2. Set up the implementation of the developed BOSI.

Integrating Equation (1) gives a relationship between the deflection angle and the fringe pattern displacement as

$$\theta_y \approx (\frac{dy}{dz}) = (\frac{\Delta y}{Z_T}) = \frac{1}{n}\int (\frac{dn}{dy})dz\,, \tag{2}$$

where θ_y is the deflection angle along the y-axis, Δy is a displacement of fringe patterns in the background plane (virtual displacement) due to the displacement of the light ray incident on the digital camera (image plane), and Z_T denotes a distance between the schlieren object and the background. The magnitude of the deflection angle in Equation (2) depends on the fringe patterns' displacements in the background plane and the refractive index gradient. The BOSI technique is thus sensitive to measuring the light ray deflection angles.

The photograph in Figure 2 shows how an implementation of the BOSI technique only needs a background pattern and a camera as the two main components. This simplicity can reduce the measurement error caused by the optical component misalignment (Raffel, 2015). A developed background was a horizontal fringe pattern in black-and-white variations printed on 30 cm × 30 cm transparent media. The thickness of each fringe was 1 mm. A white LED panel commercial was used as a light source for the background illumination. This work records the grayscale images of the BOSI technique using a Hayear model digital camera with an image resolution of 1080 pixels × 1920 pixels and a spatial resolution of 1.43 μm. A lens mounted on the digital camera was a Fujian model with a focal length of f = 50 mm. While capturing images, the lens focuses on the fringe patterns in the background. The distance between the background and the digital camera lens is Z = 1500 mm, and the distance from the background to the ultrasonic transducer head under test is Z_T = 400 mm.

A 40 cm × 40 cm filled water tank with a transparent wall provides the medium for propagating an ultrasonic wave emitted by a medical transducer head under test. The position of the tank was between the background and the camera. The technique for propagating the ultrasonic waves is to immerse the transducer head a few millimeters into the water with its face parallel to the bottom of the tank. Also, in this design, a 50 mm thick rubber slab is attached at the bottom of the tank to prevent the ultrasonic waves from back-reflecting to the transducer head face. This work tests the developed BOSI technique to visualize the ultrasonic beam of a medical therapeutic transducer operating in continuous-wave (CW) mode at a frequency of 1 MHz and an intensity of 1 W/cm^2.

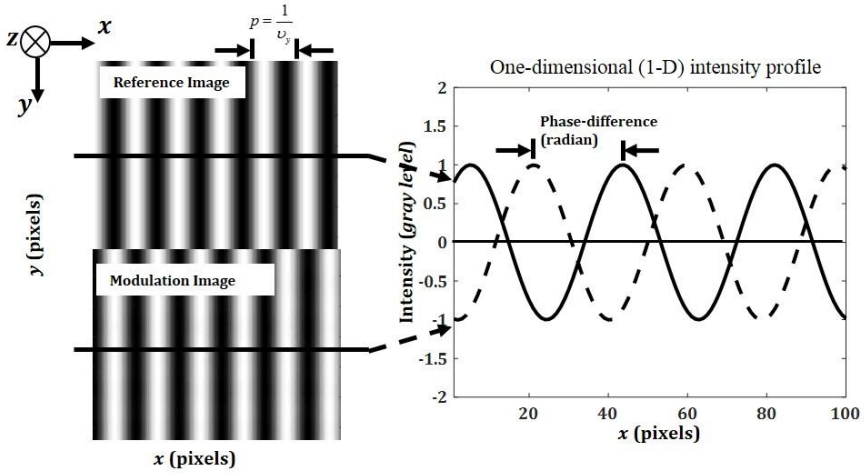

Figure 3. Illustration of a fringe pattern displacement image.

2.1 Phase Demodulation using Hilbert Transform

The propagation of ultrasonic waves in water causes a pressure wave and generates refractive index variations due to the changes in water density. The variations are similar to phase grating (grids) in the optical diffraction principle (Tian et al., 2022). When passing through the refractive index

variations or phase grating, the light rays from the background pattern diffract (deflect) at a specific angle (Figure 1). The light rays are deflected due to spatial variations in the refractive index, leading to apparent displacements in the fringe patterns. These displacements indicate a phase modulation of fringe patterns caused by the differences in optical path lengths across the refractive index variations (Zheng et al., 2021). The digital cameras in the BOSI technique capture this modulation as an image of fringe displacement relative to a reference fringe pattern (before water is exposed to ultrasonic).

Figure 3 shows an illustration of a fringe pattern displacement image. In the BOSI principle, fringe patterns can be described as sinusoidal fringe patterns that have a spatial frequency or spatial period, amplitude, and phase. Plotting the image intensity along a horizontal line across the image of fringe patterns will result in a one-dimensional (1-D) intensity profile similar to a sinusoidal signal in the spatial domain. A mathematical model can represent a sinusoidal signal in the spatial domain as (Zhu et al., 2021)

$$I_{\mathrm{R}}(x,y) = A(x,y) + B(x,y)\cos(2\pi\upsilon_y y + \varphi_{\mathrm{R}}(x,y)), \tag{3}$$

where I_{R} is the intensity distribution of the reference image along the y-axis, A is the background light intensity, B is the amplitude of light intensity describing the contrast of the fringes, υ_y is the spatial carrier (reference) frequency along the y-axis, and φ_{R} is the initial phase of reference. Similarly, a mathematical model of a phase-modulated sinusoidal fringe pattern is

$$I_{\mathrm{M}}(x,y) = A(x,y) + B(x,y)\cos(2\pi\upsilon_y y + \varphi_{\mathrm{M}}(x,y)), \tag{4}$$

where, I_{M} is the modulated intensity distribution of the modulation image along the y-axis and φ_{M} represents a phase modulation related to the physical quantity to be measured. Subtracting the phase terms in Equation (4) from Equation (3) leads to the phase difference as

$$\Delta\varphi(x,y) = \varphi_{\mathrm{M}}(x,y) - \varphi_{\mathrm{R}}(x,y), \tag{5}$$

where, $\Delta\varphi$ is the phase-difference between the reference and modulated sinusoidal fringe patterns (in rad). As stated in Equation (5), this phase difference is essential to quantify the physical information of the ultrasonic beam emitted by a transducer under test.

This work assumes that the intensity in Equation (3) and Equation (4) is real-valued data of experimental results (Zhu et al., 2021). In terms of signal theory, applying the HT to Equation (3) and Equation (4) yields an analytical signal in the complex-valued data as

$$Z(x,y) = Z_{\mathrm{RE}}(x,y) + iZ_{\mathrm{IM}}(x,y) = Z_{\mathrm{O}}(x,y)e^{i\phi(x,y)}, \tag{6}$$

where, Z is an analytical signal, Z_{RE} is the real-valued data (signal), $i = \sqrt{-1}$ is the imaginary number, Z_{IM} is imaginary-valued data, Z_{O} is the magnitude of intensity (envelope of analytical signal or amplitude), and ϕ denotes a phase of the analytical signal. Mathematically, it is convenient to obtain the phase of the analytical signal in Equation (6) as (Zhu et al., 2021)

$$\phi(x,y) = \arctan\left(\frac{Z_{\mathrm{IM}}(x,y)}{Z_{\mathrm{RE}}(x,y)}\right), \tag{7}$$

The phase signal calculated by Equation (7) is wrapped in the range $(-\pi, +\pi)$ due to the mathematical characteristics of an arctan function. Therefore, this work needs an unwrapping process to obtain the desired phase. The details of this unwrapping process are beyond the scope of this paper. In addition, using Equation (6) also gives information on the amplitude of a signal (envelope of analytical signal) as

$$\left|Z_{\mathrm{O}}(x,y)\right| = \sqrt{[Z_{\mathrm{RE}}(x,y)]^2 + [Z_{\mathrm{IM}}(x,y)]^2}, \tag{8}$$

where $\left|Z_{\mathrm{O}}\right|$ is the absolute value of signal amplitude. In this work, both Equation (7) and Equation (8) are used to visualize the ultrasonic beam.

3. RESULTS AND DISCUSSION

The raw images and comparison of the 1-D intensity profile captured by a digital camera in the BOSI technique experiment are shown in Figure 4. The principle of the BOSI technique compares the reference (Figure 4a) and modulated or modulation (Figure 4b) raw images. Once the transducer emits the ultrasonic beam, a blurred modulation image of sinusoidal fringe patterns appears at a given region, as shown in Figure 4b. As observed, the fringe patterns were distorted when compared to the raw image of reference in Figure 4a. It is strongly suspected that a blurred and distorted image indicates the presence of an ultrasonic beam emitted from a transducer head under test, as these results were also obtained by Sasono et al. (2023). As shown in Figure 4c, the image intensity distribution in column 400 (only 150 gray-level data of black dashed lines in Figure 4a and Figure 4b) reveals a comparison between the reference (blue solid curve) and modulated (modulation) intensity (black solid curve). As can be seen, there is a significant difference between the two curves. The intensity magnitude on the modulated curve decreases compared to the reference curve. This decrease in fringe contrast indicates blurring of the pattern due to light deflection from the ultrasonic-induced refractive index gradients, rather than absorption of light. In addition, it appears that the phase difference between the two curves is insignificant. Without any image processing method, the developed BOSI technique can already visually detect the presence of an ultrasonic beam. However, this result is a qualitative visual, whereas the metrology field requires both qualitative and quantitative results.

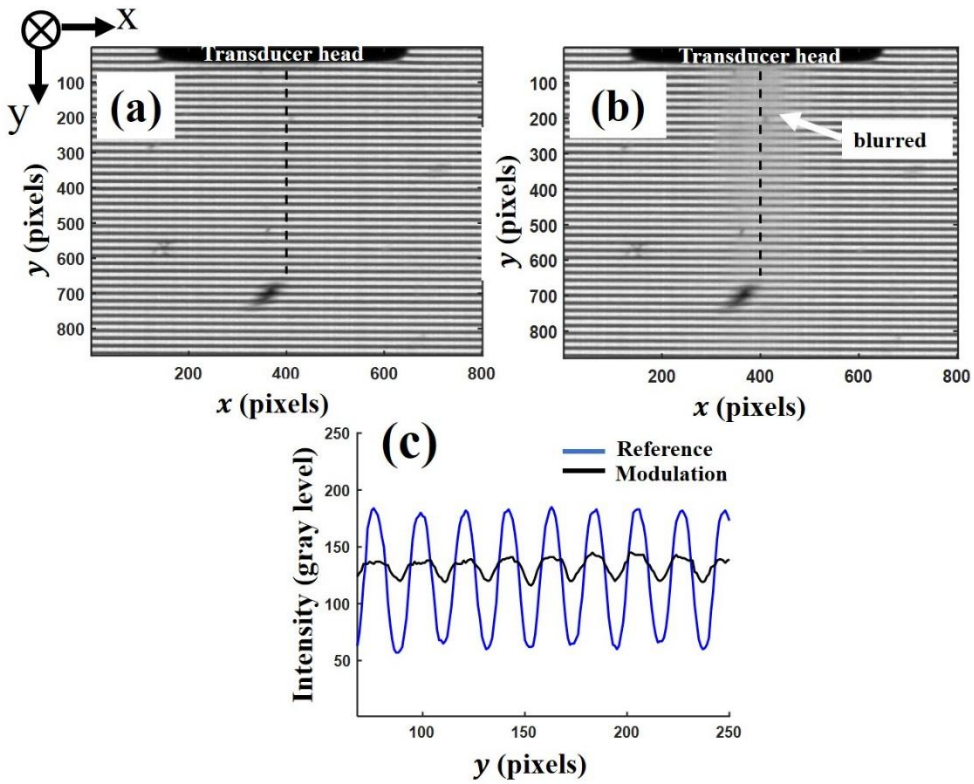

Figure 4. Raw images as captured by the camera. (a) Reference. (b) Modulation. (c) Comparison of image intensity distribution in column 400 as indicated by black dashed lines in (a) and (b).

The HT method transforms column-by-column the pixels in the raw images in Figure 4a and Figure 4b. The process is similar to scanning a raster across the image plane. As shown in Figure 5, a series of images shows the application of the HT method for extracting the phase in the BOSI images. All computations in this work use a MATLAB environment. A MATLAB 'hilbert' function transforms the image intensity distribution in Figure 4a and Figure 4b into the complex-valued data (analytical

signal). Next, the MATLAB 'arctan' function calculates the wrapped phase of the reference and modulation images of sinusoidal fringe patterns, as shown in Figure 5a and Figure 5b, respectively.

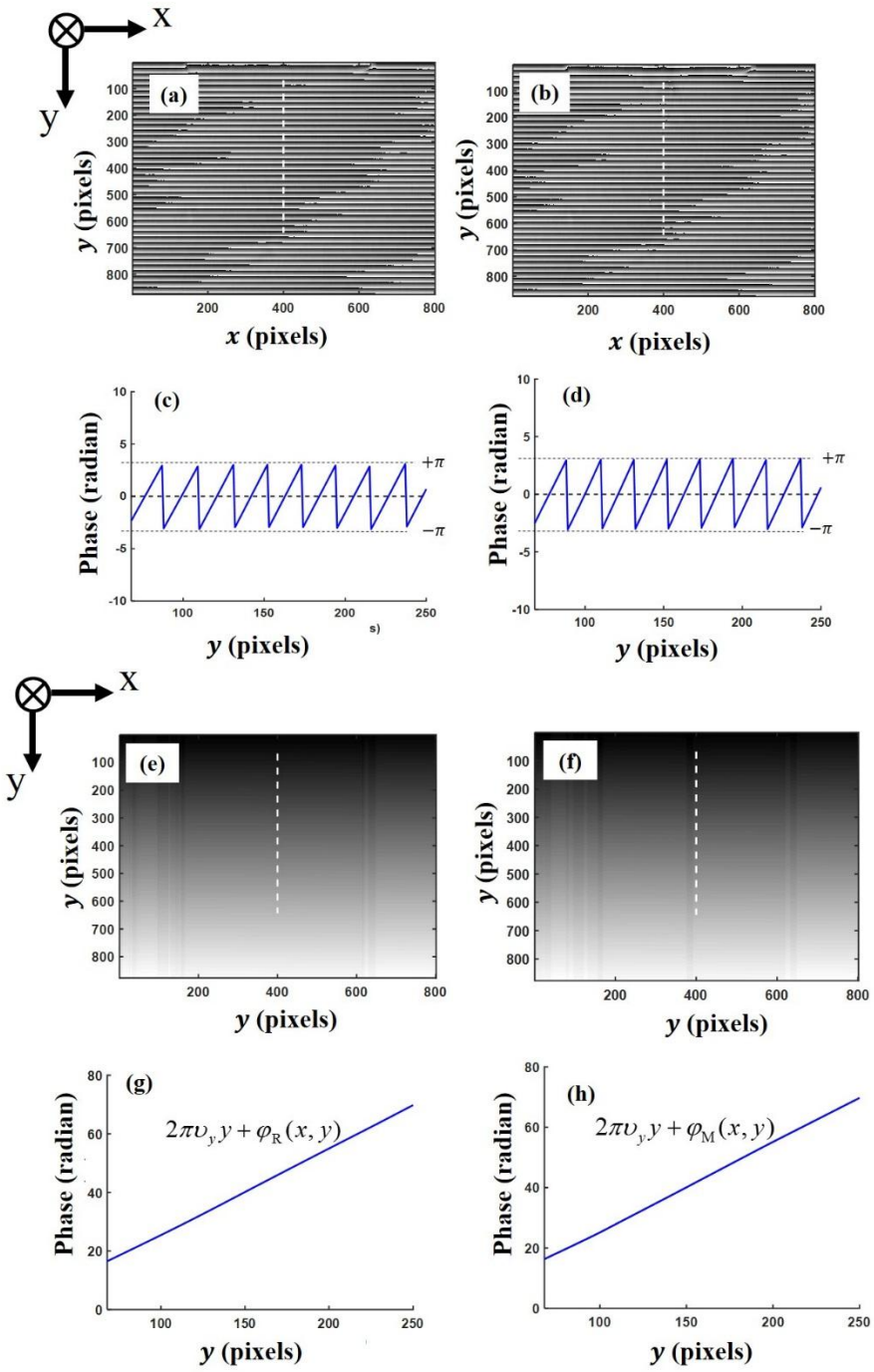

Figure 5. Extracting phase of raw images using the HT method. (a) Wrapped phase of the reference image. (b) Wrapped phase of the modulation image. Wrapped phase curves of reference (c) and modulation (d) in column 400 as indicated by white dashed lines in figures (a) and (b). (e) Unwrapped phase of the reference image. (f) Unwrapped phase of the modulation image. Unwrapped phase curves of reference (g) and modulation (h) in column 400 as indicated by white dashed lines in (e) and (f).

The phase distributions in column 400 (a segment of white dashed lines in Figure 5a and Figure 5b) show the wrapped phase curves in the range $(-\pi, +\pi)$ of reference (Figure 5c) and modulation

(Figure 5d) according to Equation (7). The unwrapping process using MATLAB's 'unwrap' function of Figure 5a and Figure 5b leads to the unwrapped phase images, as shown in Figure 5e (reference) and Figure 5f (modulation). The phase distributions in column 400 (a segment of white dashed lines in Figure 5e and Figure 5f) show the unwrapped phase curves of reference (Figure 5g) and modulation (Figure 5h). As observed, the curves of the unwrapped phase have spatially linear characteristics according to Equation 3 and Equation 4. These results are consistent with those obtained by Meng et al. (2022).

As shown in Figure 6a, subtracting the unwrapped phase in Figure 5f from Figure 5e yields an image of phase difference related to the 2-D physical characteristics of the density changes in water due to the propagation of the ultrasonic beam. As observed, the image reveals the bright-dark variations (brightness variations as indicated by the arrows). The bright intensity in Figure 6a can be expected to have high water density. Conversely, dark intensity can indicate low water density. Thus, periodic variations of the phase difference can describe changes in water density, which in turn visualizes the ultrasonic beam. The previous results have consistently obtained that the variation in phase difference is proportional to the variation in ultrasonic pressure amplitude (ultrasonic beam), as demonstrated by Pulkkinen et al. (2017), Luo et al. (2020) and Ichihara et al. (2025).

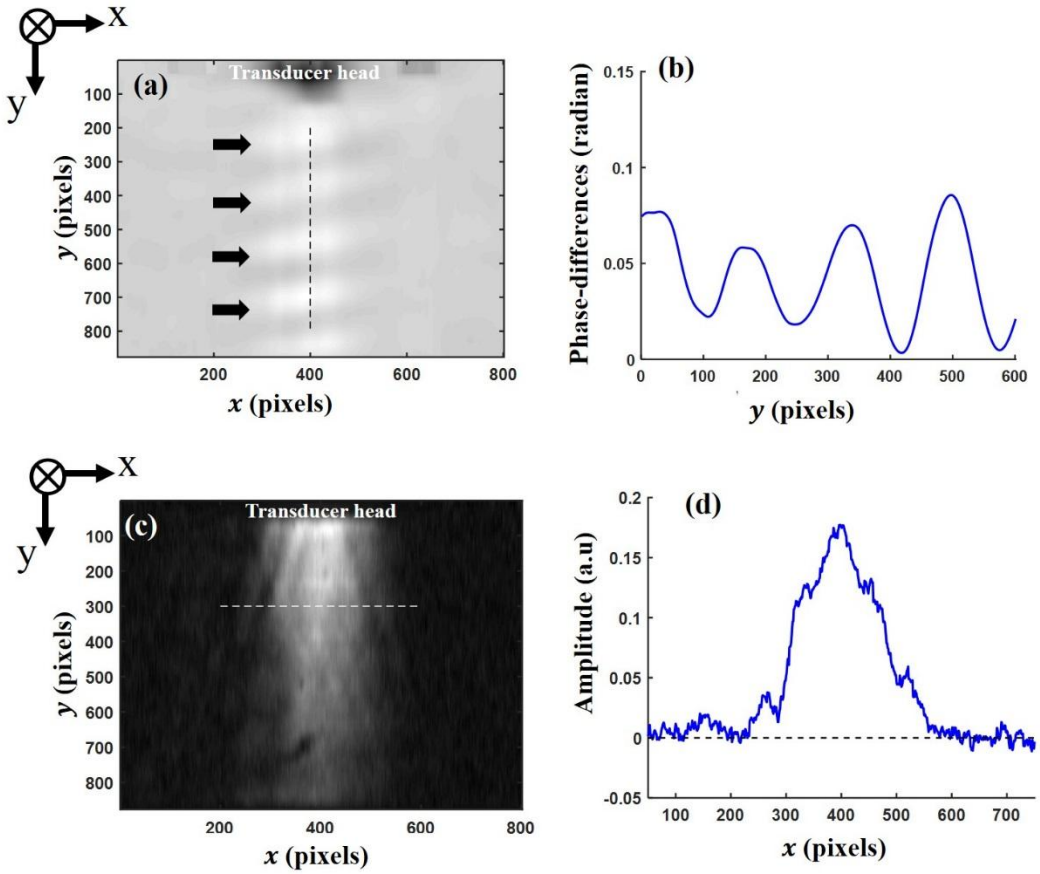

Figure 6. (a) Reconstructed phase-difference image. (b) Plot of phase-difference data along black dashed lines (y-position in column 400). (c) Reconstructed amplitude image. (d) Plot of amplitude data along white dashed lines (x-position in row 300).

As shown in Figure 6b, the phase-difference data of column 400 along the black dashed lines in Figure 6a reveal an undulation curve similar to the physical characteristics of a harmonic wave. This undulation may be related to the compression and rarefaction of water density under the influence of ultrasonic pressure waves, as outlined in the principle of a sound wave outlined in (Goldfain et al., 2021). On the other side, Figure 6c shows an amplitude image obtained by the HT method. Visually, there is a

significant difference between the phase-difference image (Figure 6a) and the amplitude image (Figure 6c). The phase-difference image describes variations of the apparent fringe phase related to the changes in water density. On the other hand, the amplitude image represents the light intensity as captured by a conventional camera. As shown in Figure 6d, the amplitude data of row 300 along the white dashed lines in Figure 6c reveal a curve of the Hilbert amplitude distribution, providing a measure of local fringe contrast. While not quantitatively proportional to ultrasonic beam intensity, it qualitatively reflects regions of stronger refractive index gradients and thus higher ultrasonic influence. As shown in Figure 6d, the curve is similar to a Gaussian shape that exhibits high intensity at the centre of the transducer head under test. The curve width can be related to the ultrasonic beam width, as outlined in (Zeng et al., 2022). Therefore, both curves (Figure 6b and Figure 6d) can be the basis for obtaining detailed physical information about the ultrasonic waves emitted from a transducer head under test.

4. CONCLUSION

This paper has successfully developed the BOSI technique by using the proposed sinusoidal fringe pattern background (instead of random dots) combined with the HT method to visualize the ultrasonic beam emitted by a medical (therapeutic) transducer head under test. The developed BOSI technique successfully converts the fringe pattern displacements in the background into the phase-difference and amplitude data. The BOSI technique then reconstructs the data into the images representing an ultrasonic beam. The result also shows that the phase-difference and amplitude images differ significantly. However, both images can be essential for obtaining detailed physical information about the ultrasonic beam of a medical transducer. The developed BOSI offers the advantages of simple, rapid, 2-D visualization and non-intrusive techniques. Hence, the developed BOSI technique has the potential to improve the calibration of ultrasonic waves emitted from the transducers, particularly for medical transducers.

ACKNOWLEDGEMENT

We would like to thank the lab assistants of Advanced Laboratory Physics (AloP)-Study Program Physics of Ahmad Dahlan University (UAD) for the experimental setup and technical assistance in image capture with the CCD Camera.

REFERENCE

Akiyama, I. (2020). Basic and recent applied technologies of ultrasound in the field of clinical diagnosis. *Acoustical Science and Technology*, *41*(6), 845–850. https://doi.org/10.1250/ast.41.845

Colom, M., Ricci, P., & Duocastella, M. (2023). Rapid quantification of 3D ultrasound fields with wavefront sensing and Schlieren tomography. *Ultrasonics*, *135*(April), 107115. https://doi.org/10.1016/j.ultras.2023.107115

Ding, H., Yi, S., & Zhao, X. (2019). Experimental investigation of aero-optics induced by supersonic film based on near-field background-oriented schlieren. *Applied Optics*, *58*(11), 2948. https://doi.org/10.1364/ao.58.002948

Draper, D., & M Mallipudi, R. (2020). Therapeutic ultrasound: myths and truths for nonportable in-clinic and portable home use ultrasound. *MOJ Sports Medicine*, *4*(4), 115–116. https://doi.org/10.15406/mojsm.2020.04.00107

Dunlap, M. D., Beach, J., & Massey, T. (2020). Ultrasound beam characterization through real time visualization with schlieren imaging. *IEEE International Ultrasonics Symposium, IUS*, *2020-Septe*, 0–3. https://doi.org/10.1109/IUS46767.2020.9251685

Goldfain, A. M., Yung, C. S., Briggman, K. A., & Hwang, J. (2021). Optical phase contrast imaging for absolute, quantitative measurements of ultrasonic fields with frequencies up to 20 MHz. *The Journal of the Acoustical Society of America*, *149*(6), 4620–4629. https://doi.org/10.1121/10.0005431

Grauer, S. J., & Steinberg, A. M. (2020). Fast and robust volumetric refractive index measurement by unified background-oriented schlieren tomography. *Experiments in Fluids*, *61*(3). https://doi.org/10.1007/s00348-020-2912-1

Harris, G. R., Howard, S. M., Hurrell, A. M., Lewin, P. A., Schafer, M. E., Wear, K. A., Wilkens, V., & Zeqiri, B. (2023). Hydrophone Measurements for Biomedical Ultrasound Applications: A Review. *IEEE Transactions on Ultrasonics, Ferroelectrics, and Frequency Control*, *70*(2), 85–100. https://doi.org/10.1109/TUFFC.2022.3213185

Hofmann, M., Haeberlin, A., de Brot, S., Stahel, A., Keppner, H., & Burger, J. (2023). Development and evaluation of a titanium-based planar ultrasonic scalpel for precision surgery. *Ultrasonics*, *130*(May 2022), 106927. https://doi.org/10.1016/j.ultras.2023.106927

Ichihara, S., Yamagishi, M., Kurashina, Y., Ota, M., & Tagawa, Y. (2025). High-resolution pressure imaging via background-oriented schlieren tomography: A spatiotemporal measurement for MHz ultrasound fields and hydrophone calibration. *Ultrasonics*, *152*(February), 107614. https://doi.org/10.1016/j.ultras.2025.107614

Kaneko, Y., Nishida, H., & Tagawa, Y. (2021). Background-oriented schlieren measurement of near-surface density field in surface dielectric-barrier-discharge. *Measurement Science and Technology*, *32*(12). https://doi.org/10.1088/1361-6501/ac1ccc

Koponen, E., Leskinen, J., Tarvainen, T., & Pulkkinen, A. (2022). Nonlinear estimation of pressure projection of ultrasound fields in background-oriented schlieren imaging. *Journal of the Optical Society of America A*, *39*(4), 552. https://doi.org/10.1364/josaa.433762

Luo, H., Kusunose, J., Pinton, G., Caskey, C. F., & Grissom, W. A. (2020). Rapid quantitative imaging of high intensity ultrasonic pressure fields. *The Journal of the Acoustical Society of America*, *148*(2), 660–677. https://doi.org/10.1121/10.0001689

Meinecke, M., Kilzer, A., & Weidner, E. (2020). Background Orientated Schlieren Method Applied for Liquid Systems of Strong Refractive Gradients. *Chemie-Ingenieur-Technik*, *92*(8), 1089–1097. https://doi.org/10.1002/cite.201900189

Meng, X., Wang, F., Liu, J., Chen, M., & Wang, Y. (2022). Phase shifting profilometry based on Hilbert transform: An efficient phase unwrapping algorithm. *Journal of Applied Physics*, *131*(19). https://doi.org/10.1063/5.0084695

Mizukaki, T., Odagiri, T., Matsumura, T., & Wakabayashi, K. (2020). Quantitative flow visualization of a blast wave from an underground magazine model using backgroundoriented schlieren. *Sci. Tech. Energetic Materials*, *81*(5), 128–136.

Nienhaus, F., Piotrowski, T., Nießing, B., König, N., & Schmitt, R. H. (2023). Adaptive phase contrast microscopy to compensate for the meniscus effect. *Scientific Reports*, *13*(1), 1–11. https://doi.org/10.1038/s41598-023-32917-6

Pulkkinen, A., Leskinen, J. J., & Tiihonen, A. (2017). Ultrasound field characterization using synthetic schlieren tomography. *The Journal of the Acoustical Society of America*, *141*(6), 4600–4609. https://doi.org/10.1121/1.4986623

Raffel, M. (2015). Background-oriented schlieren (BOS) techniques. *Experiments in Fluids*, *56*(3), 1–17. https://doi.org/10.1007/s00348-015-1927-5

Sasono M., Setyawan P.Sakti, J. E. N. and H. S. (2023). Visualization of Therapeutic Ultrasound Beams U sing. *AIP Conference Proceedings*, *March 2019*.

Shen, B., Zeng, B., Liu, X., Feng, C., Hu, Z., Hu, J., & Zhu, F. (2021). Accuracy optimization method of ultrasonic power measurement system based on acousto-optic effect. *Optical Review*, *28*(2), 207–214. https://doi.org/10.1007/s10043-021-00651-x

Tian, L., Shen, Q., & Chang, H. (2022). A novel progressive wave gyroscope based on acousto-optic effects. *Microsystems and Nanoengineering*, *8*(1). https://doi.org/10.1038/s41378-022-00429-4

Vinnichenko, N. A., Pushtaev, A. V., Plaksina, Y. Y., & Uvarov, A. V. (2023). Performance of Background Oriented Schlieren with different background patterns and image processing techniques. *Experimental Thermal and Fluid Science*, *147*(April), 110934. https://doi.org/10.1016/j.expthermflusci.2023.110934

Wei, L., Qi, H., Li, G., Ruan, S. T., & Li, H. (2021). Tomographic reconstruction of refractive index fields based on laser beam deflection measurement. *Optics Communications*, *492*(March), 126951. https://doi.org/10.1016/j.optcom.2021.126951

Xing, G., Wilkens, V., & Yang, P. (2021). Review of field characterization techniques for high intensity therapeutic ultrasound. *Metrologia*, *58*(2). https://doi.org/10.1088/1681-7575/abe02e

Yamagishi, M., Yahagi, Y., Ota, M., Hirose, Y., Udagawa, S., Inage, T., Kubota, S., Fujita, K., Ohtani, K., & Nagai, H. (2021). Quantitative density measurement of wake region behind reentry capsule (Improvements in accuracy of 3D reconstruction by evaluating the view-angle of measurement system). *Journal of Fluid Science and Technology*, *16*(3), 1–10. https://doi.org/10.1299/jfst.2021jfst0021

Zeng, K., Darmani, G., Fomenko, A., Xia, X., Tran, S., Nankoo, J. F., Shamli Oghli, Y., Wang, Y., Lozano, A.

M., & Chen, R. (2022). Induction of Human Motor Cortex Plasticity by Theta Burst Transcranial Ultrasound Stimulation. *Annals of Neurology*, *91*(2), 238–252. https://doi.org/10.1002/ana.26294

Zheng, H. kun, Lv, R. qing, Zhao, Y., Wang, X. xin, Lin, Z. ting, Zhou, Y. fan, & Zhao, Q. (2021). A novel high accuracy optical path difference compensation method based on phase difference technology. *Optics and Lasers in Engineering*, *137*(July 2020), 106367. https://doi.org/10.1016/j.optlaseng.2020.106367

Zhu, J., Wu, Y., Yue, H., & Shao, X. (2021). Single frame phase estimation based on Hilbert transform and Lissajous Ellipse Fitting method in fringe projection technology. *Optics Communications*, *488*(January), 126817. https://doi.org/10.1016/j.optcom.2021.126817